2019 IEEE PES/IAS PowerAfrica

Multi-type FACTS Location and Coordination using PI-PSO for Transfer Capability Improvement

Ahmad Abubakar Sadiq
Electrical and Electronics Engineering
Federal University of Technology
Minna, Nigeria
ahmad.abubakar@futminna.edu.ng

Sunusi Sani Adamu
Muhammad Buhari
Electrical Engineering
Bayero University
Kano, Nigeria

***Abstract*— Deregulation ensures competition amongst utilities through open access regulation to accommodate a significant increase in the volume of power transactions. However, this action may cause line overloads and congestion. To relief congestion, improved utilization and performance of transmission infrastructure, different types of FACTS devices are planned with diverse objectives. Often the huge investment cost of FACTS leads to the implementation of a single type of FACTS' planning by utilities at a given time horizon. To optimize performance, subsequent planning must take into account and coordinate with the existing FACTS regarding location and parameter settings. This article proposed a real power flow Performance Index (PI) and Particle Swarm Optimization (PSO) to locate and coordinate Static synchronous series compensator (SSSC) with an existing Thyristor control series compensator (TCSC) in a standard 9-buses test network. Results of three coordination schemes show that the scheme with more decision parameters provides superior loadability and transfer capability improvement.**

***Index Terms*—FACTS' Coordination, Power Transaction, Particle Swarm Optimization, Transmission grid, Transfer Capability.**

I. INTRODUCTION

Deregulation ensures competition amongst utilities through open access to the transmission grid; whereas the ability of the grid to accommodates a high volume of power transactions while ensuring power system's security is a major concern [1]. The open access feature, if not adequately managed can cause power flow overloads and congestion which leads to instability [2].

The economic and regulatory constraints on transmission network expansion and new right of ways cause a reduction in stability margins, voltage issues and increased risk of cascading outages in the presence of unmanaged power transactions [3], [4]. Utilities, therefore, seek to maximise the utilisation of the existing transmission infrastructure. One approach is through optimal deployment of Flexible Alternating Current Transmission Systems (FACTS) devices. FACTS technology enables power flow re-distribution through the use of circuit parameters to mitigate overload and congestion [5]. Conversely, the high investment cost practically constrained utilities to a single type of FACTS planning at a given time horizon [6]. However, subsequent planning must take into account and coordinate with the existing FACTS regarding location and parameter settings to optimise performance. Consequently, multiple FACTS planning at different time horizon requires adequate coordination of decision parameters for improved performance.

Reference [6] proposes an approach to allocate multi-type FACTS within the same time horizon. [7]–[10] present multiple SVC, TCSC and their combination to enhance ATC; since the same planning horizon is assumed, SVC and TCSC's coordination is ignored. ATC enhancement with multiple STATCOM, SSSC and UPFC separately were demonstrated in [11] under the same time horizon. Also in [12], TTC enhancement is demonstrated with multi-type FACTS consisting of TCSC, TCPS, SVC and UPFC simultaneously, which is rare in practice.

In practice, each FACTS device allows two degrees of freedom as decision parameter: location and size, at a given planning horizon. However, in a successive time horizon, the degree of freedom reduces by one (that is the location of an existing FACTS) due to the bulkiness of FACTS. The methodology adopted differs from multiple FACTS planning in a single time horizon which ignores coordination of existing FACTS' parameter. This article demonstrates coordination of SSSC with an existing TCSC and compares three coordination scenarios under successive planning horizon.

II. STATIC MODELLING OF FACTS

A. TCSC modeling

Fig. 1 depicts a transmission line with TCSC modelled by reactance jx_k. Equation (1) gives the equivalent line reactance with TCSC.

$$x_{ij}^{new} = x_{ij} - x_k \tag{1}$$

Using Power injection model (PIM), TCSC is modelled by power injections at the terminal buses, as shown in Fig. 2.

Supported by Petroleum Technology Development Funds (PTDF), Nigeria. Under scholar no. PTDF/ED/LSS/PHD/AAS/118/17

978-1-7281-1010-3/19/$31.00 ©2019 IEEE

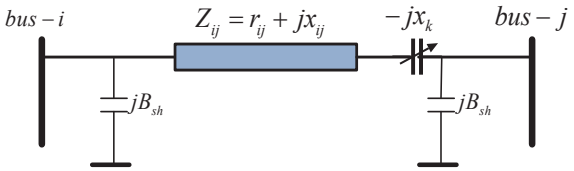

Fig. 1.Transmission line Model with TCSC

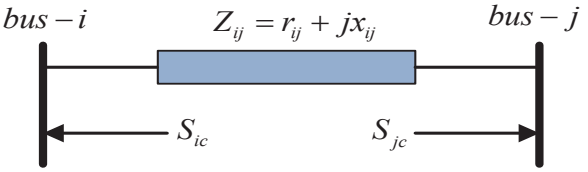

Fig. 2. Power Injection Model of TCSC

Equations (2) to (5) describes the power injections while equations (6) and (7) gives the changes in conductance and susceptance; δ_{ij} is the voltage angular difference between the ith and jth buses; $\Delta Y_{ij} = \Delta G_{ij} + \Delta B_{ij}$ is line admittance [13].

$$P_{ic} = V_i^2 \Delta G_{ij} - V_i V_j \left(\Delta G_{ij} \cos\delta_{ij} + \Delta B_{ij} sin\delta_{ij} \right) \quad (2)$$

$$Q_{ic} = -V_i^2 \Delta B_{ij} - V_i V_j \left(\Delta G_{ij} \sin\delta_{ij} - \Delta B_{ij} \cos\delta_{ij} \right) \quad (3)$$

$$P_{jc} = V_j^2 \Delta G_{ij} - V_j V_i \left(\Delta G_{ij} \cos\delta_{ij} - \Delta B_{ij} sin\delta_{ij} \right) \quad (4)$$

$$Q_{jc} = -V_j^2 \Delta B_{ij} + V_j V_i \left(\Delta G_{ij} \sin\delta_{ij} + \Delta B_{ij} \cos\delta_{ij} \right) \quad (5)$$

$$\Delta G_{ij} = \frac{x_k r_{ij} \left(x_k - 2x_{ij} \right)}{\left(r_{ij}^2 + x_{ij}^2 \right) \left(r_{ij}^2 + (x_{ij} - x_k)^2 \right)} \quad (6)$$

$$\Delta B_{ij} = \frac{-x_k (r_{ij}^2 - x_{ij}^2 + x_k x_{ij})}{\left(r_{ij}^2 + x_{ij}^2 \right) \left(r_{ij}^2 + (x_{ij} - x_k)^2 \right)} \quad (7)$$

B. SSSC modeling

Fig. 3 shows the equivalent SSSC circuit, modelled by a voltage source $V_{se}\angle\delta_{se}$ connected in series with impedance z_{se} to account for coupling transformer losses. Using Norton equivalent, the PIM equivalent of SSSC is modelled by complex loads at buses i and n as shown in Fig. 4. Equations (8) and (9) gives the SSSC's complex power injections [14].

$$S^i_{inj} = P^{ic}_{inj} + jQ^{ic}_{inj} = \overline{V_i} (I_{inj})^* \quad (8)$$

$$S^n_{inj} = P^n_{inj} + jQ^n_{inj} = -\overline{V_n} (I_{inj})^* \quad (9)$$

III. Sensitivity of Real Power Flow Performance Index

Power flow congestion is a major constraints to power transfer [15], hence the sensitivity of active power flows to circuit parameter measures the suitability of FACTS location in a candidate line to redistribute power flow and relieve

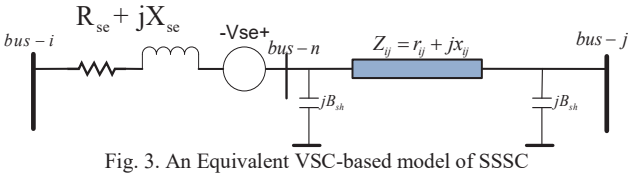

Fig. 3. An Equivalent VSC-based model of SSSC

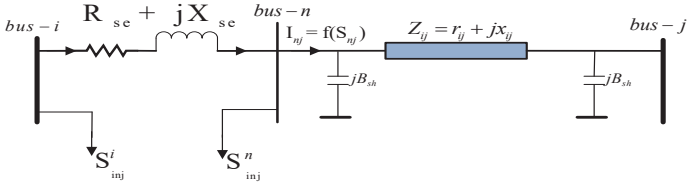

Fig. 4. Power Injection Model of SSSC

congestion. Equation (10) gives the second order real power flow performance indices (PI_2).

Accordingly, when power flow congestion limits' power transfer transaction, equation (11) evaluate the sensitivity of PI_2 to FACTS' control parameters (X_{FACTS}) [16].

$$PI_2 = \sum_{m=1}^{N_L} \frac{w_m}{2n} \left(\frac{P_{lm}}{P_{lm}^{\max}} \right)^{2n} \quad (10)$$

$$\frac{\partial PI_2}{\partial X_{facts}} = \sum_{m=1}^{N_L} w_m P_{lm}^{(2n-1)} \left(\frac{1}{P_{lm}^{\max}} \right)^{2n} \frac{\partial P_{lm}}{\partial X_{facts}} \quad (11)$$

In equations (10) and (11), N_L is the number of lines, $W_m = 1$, is non-negative weight coefficient use to reflect the importance of the line, n is the n-exponent order, P_{lm} is active power flow, and P^{max} is the rated capacity of the line. Equation (12) expresses the active power flow P_{lm} as the sum of real power injections [13].

$$P_{lm} = \begin{cases} \sum_{n=1, n \neq s}^{nb} S_{mn} P_n & for\ m \neq k \\ \sum_{n=1, n=s}^{nb} S_{mn} P_n + P_j & for\ m = k \end{cases} \quad (12)$$

In equation (12), s is the slack bus; nb is the number of buses in the network, S_{mn} is the mnth element of the matrix [$\mathbf{S_f}$] that relates line power flows with bus power injections at the buses without FACTS. Equation (13) expresses the partial derivative of the active power flow of equation (12) [16].

$$\frac{\partial P_{lm}}{\partial X_k} = \begin{cases} \left(S_{mi} \frac{\partial P_i}{\partial X_k} + S_{mj} \frac{\partial P_j}{\partial X_k} \right) & for\ m \neq k \\ \left(S_{mi} \frac{\partial P_i}{\partial X_k} + S_{mj} \frac{\partial P_j}{\partial X_k} \right) + \frac{\partial P_j}{\partial X_k} & for\ m = k \end{cases} \quad (13)$$

For TCSC, the derivative terms in equation (13) are the partial derivative of equations (2) and (4) which models the TCSC as power injections. Equations (14) to (17) expresses the derivative with respect to TCSC's reactance.

$$\left.\frac{\partial P_i}{\partial X_k}\right|_{x_k=0}=\left.\frac{\partial P_{ic}}{\partial x_k}\right|_{x_k=0}=(V_i^2-V_iV_j\cos\delta_{ij})\left.\frac{\partial \Delta G_{ij}}{\partial X_k}\right|_{x_k=0}-(V_iV_j\sin\delta_{ij})\left.\frac{\partial \Delta B_{ij}}{\partial X_k}\right|_{x_k=0} \quad (14)$$

$$\left.\frac{\partial P_j}{\partial X_k}\right|_{x_k=0}=\left.\frac{\partial P_{jc}}{\partial x_k}\right|_{x_k=0}=(V_j^2-V_iV_j\cos\delta_{ij})\left.\frac{\partial \Delta G_{ij}}{\partial X_k}\right|_{x_k=0}+(V_iV_j\sin\delta_{ij})\left.\frac{\partial \Delta B_{ij}}{\partial X_k}\right|_{x_k=0} \quad (15)$$

$$\left.\frac{\partial \Delta G_{ij}}{\partial x_k}\right|_{x_k=0}=2G_{ij}B_{ij} \quad (16)$$

$$\left.\frac{\partial \Delta B_{ij}}{\partial x_k}\right|_{x_k=0}=B_{ij}^2-G_{ij}^2 \quad (17)$$

For the SSSC, the derivative terms in equation (13) are the partial derivative of the real part of equations (8) and (9) which models the SSSC as power injections. Equations (18) and (19) gives the derivative with respect to the magnitude of the series injected voltage of SSSC.

$$\left.\frac{\partial P_i}{\partial X_k}\right|_{x_k=0}=\left.\frac{\partial P_{inj}^{ic}}{\partial V_{se}}\right|_{V_{se}=0}=V_i\left[G_{se}\cos(\delta_i+\delta_{se})-B_{se}\sin(\delta_i+\delta_{se})\right] \quad (18)$$

$$\left.\frac{\partial P_j}{\partial X_k}\right|_{x_k=0}=\left.\frac{\partial P_{inj}^{nc}}{\partial V_{se}}\right|_{V_{se}=0}=-V_n\left[G_{se}\cos(\delta_n+\delta_{se})-B_{se}\sin(\delta_n+\delta_{se})\right] \quad (19)$$

Note that in equations (14) to (19), the sensitivities are obtained by assuming that $X_{FACTS}\to 0$.

IV. Continuation Power Flow (CPF)

Normally, CPF varies load and generation simultaneously, by a loading parameter λ to parameterise and solves the power flow equations using a predictor-corrector scheme, thereby avoid ill-conditioning and singularity. The high accuracy and efficiency of CPF make it one of the widely used methods for static security assessment [17].

Comprehensive documentation of CPF for Available Transfer Capability (ATC) evaluation are given in [18]–[20]. At a maximum loading parameter resulting from an imposed constraints, evaluation of ATC with FACTS formulates to an optimisation objective expressed by equation (20) [21].

$$\text{Maximise}\left\{ATC=\sum_{i\in sink}P_L^i(\lambda_{limited})-\sum_{i\in sink}P_L^i(\lambda=0)\right\} \quad (20)$$

Subject to,

$$f(x,\lambda)=0 \quad (21)$$

$$0\le\lambda\le\lambda_{limited} \quad (22)$$

$$P_g^{\min}\le P_g\le P_g^{\max} \quad (23)$$

$$Q_g^{\min}\le Q_g\le Q_g^{\max} \quad (24)$$

$$S_{ij}\le S_{ij}^{rated} \quad (25)$$

$$V_i^{\min}\le V_i\le V_i^{\max} \quad (26)$$

$$X_{FACTS}^{\min}\le X_{FACTS}\le X_{FACTS}^{\max} \quad (27)$$

Equation (21) is the nonlinear compact power flow equation, with state variable x = (V; δ) as voltage magnitude and angle. In equations (22) to (26), $\lambda_{limited}$, P_g, Q_g, S_{ij}, and V_i are loading parameter, real, reactive, apparent power flows and voltage magnitude respectively. Equation (27) ensures minimum FACTS' size which is treated as a constraint and imposed by X_{FACTS}; $-0.8\le X_{TCSC}\le 0.2$ for TCSC, and $0\le X_{SSSC}\le 0.1$ for SSSC respectively.

V. Hybrid Performance Index and Particle Swarm Optimization (PI – PSO)

In the proposed PI-PSO, ∂PI obtains a vector of potential candidate location of FACTS within which PSO optimise the size, thereby improves overall algorithm exploitation ability and avoid local optimal solutions. Particle's position is described by equation (28), such that λ and X are location and size respectively. For an m-dimension candidate location vector, in addition to position and velocity updates of equations (29) and (30) respectively in traditional PSO, position update in the proposed PI-PSO is described in equation (31).

$$\eta_i^k=\left[\lambda_i^k, X_i^k\right] \quad (28)$$

$$\eta_i^{k+1}=\eta_i^k+V_i^{k+1} \quad (29)$$

$$V_i^{k+1}=\omega V_i^k+c_1 rand(Pbest_i^k-\eta_i^k)+c_2 rand(Gbest_i^k-\eta_i^k) \quad (30)$$

$$X_i^{k+1}=\begin{cases}X_i^{k+1}(\lambda_i) & if\ \lambda_i^{k+1}\in\mathbb{N}\\ \mathbb{N} & \mathbb{N}\\ X_i^{k+1}(\eta_i) & for\ \eta_i\in\mathbb{R}\end{cases} \quad (31)$$

VI. Coordination Schemes

The term coordination implies that FACTS' decision parameters have been tuned simultaneously for an overall improvement of the objective. Planning of TCSC and SSSC under successive time horizons requires the coordination of four decision parameters namely $[\lambda_{TCSC}, X_{TCSC}, \lambda_{SSSC}, X_{SSSC}]$. Since multiple FACTS planning within the same time horizon is rare in practice, consequently three coordination scenarios of SSSC with an existing TCSC is planned using PI-PSO under successive planning horizons. As a strategy, multiple FACTS on the same location is precluded. The three coordination schemes are described as follows:

A. Scheme_1

X_{SSSC} coordinates only with the variable X_{TCSC}: Locations of TCSC and SSSC optimally planned separately using PI-PSO are retained, while PSO optimises their sizes at these respective locations. The decision variables are $[X_{TCSC}, X_{SSSC}]$.

B. Scheme_2

λ_{SSSC} *and* X_{SSSC} coordinates with static λ_{TCSC} *and* X_{TCSC}: SSSC's location and size are optimised in the presence of an optimally planned (location and size) TCSC separately using PI-PSO. The decision variables are $[\lambda_{SSSC}, X_{SSSC}]$.

C. Scheme_3

λ_{SSSC} *and* X_{SSSC} coordinates with static λ_{TCSC} and variable X_{TCSC}. This scheme optimises the location and size of SSSC as well as the size of a separately planned TCSC using PI-PSO. The decision variables are $[X_{TCSC}, \lambda_{SSSC}, X_{SSSC}]$.

VII. Results and Discussion

Fig. 5 depicts the one-line diagram of the Western System Coordinating Council (WSCC) 9 buses network obtained by a web-based network visualisation tool "stac" (Steady-State AC Network Visualization in the Browser).

Several multilateral power transactions were simulated with the proposed method in MATPOWER environment. Transfer

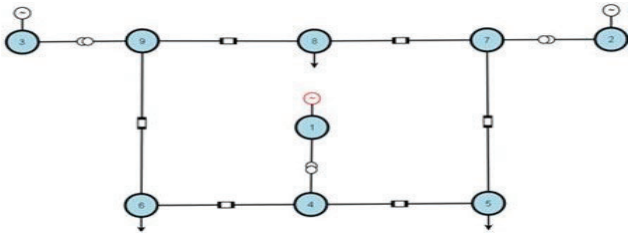

Fig. 5. One-line diagram of WSCC 9 buses

directions of some transactions are described in the 2nd and 3rd column of Table I.

The sensitivities of real power flow to TCSC and SSSC's control parameters to each transaction is given in Tables I and II respectively. The elements of the vector which constitutes the potential candidate locations of TCSC and SSSC are in bold.

For each transaction, the enhance ATC values with TCSC and SSSC using the proposed PI-PSO are given Tables III, while Fig. 6 shows the convergence curve for T4 with SSSC using PSO and PI-PSO.

TABLE I. Sensitivity of PI to TCSC's Reactance

Trans ID	Transfer direction		Line number (terminating buses)								
	Source	Sink	1(1 to 4)	2(4 to 5)	3(5 to 7)	4(2 to 7)	5(7 to 8)	6(8 to 9)	7(9 to 3)	8(9 to 6)	9(6 to 4)
T1	1,3	5	0.0137	-0.7046	1.7751	0.0898	-0.1183	0.6834	-0.0484	**-0.9763**	**-0.0192**
T2	1,2	5,8	-0.0273	0.2582	**-0.5396**	-0.0268	*0.9141*	**-0.1696**	0.0368	0.4394	**-0.4586**
T3	1,2,3	5,6	0.0772	0.0314	*1.298*	0.0765	**-0.3613**	0.0104	-0.0322	**-0.5668**	0.3071
T4	1,2,3	6,8	-0.0696	**-0.191**	**-0.4354**	-0.0201	*0.8763*	**-0.1804**	0.098	0.8005	**-0.6959**
T5	1,2,3	5,8	-0.0586	0.7089	**-0.1627**	0.0104	*1.1636*	**-1.0226**	-0.006	0.0126	**-1.5384**

TABLE II. Sensitivity of PI to TCSC's Reactance

Trans ID	Transfer direction		Line number (terminating buses)								
	Source	Sink	1(1 to 4)	2(4 to 5)	3(5 to 7)	4(2 to 7)	5(7 to 8)	6(8 to 9)	7(9 to 3)	8(9 to 6)	9(6 to 4)
T1	1,3	5	-0.057	3.4411	**-5.329**	0.5169	0.4379	**-3.3775**	-0.2709	5.117	0.0364
T2	1,2	5,8	-0.0841	**-1.088**	4.6866	2.2759	**-3.5912**	0.9938	-0.097	**-1.9424**	2.554
T3	1,2,3	5,6	-0.2885	**-0.0964**	**-2.6338**	1.6763	2.5468	**-0.1333**	-0.0142	3.3301	**-1.3878**
T4	1,2,3	6,8	0.2544	1.0153	4.4098	2.4144	**-3.2473**	1.018	-0.3463	**-3.5896**	3.9137
T5	1,2,3	5,8	-0.1154	**-0.0411**	0.436	2.4735	1.2911	**-0.0552**	-0.1271	0.3864	0.0022

From Table III, observe that ATC improvement is achieved with the optimal location of TCSC and SSSC individually using PI-PSO. Furthermore, Fig. 6 depicts an improve exploitation ability of PI-PSO over the conventional PSO regarding the starting point and convergence to global optima.

Tables IV, V and VI gives the ATC and optimal multi-type FACTS' decision parameters for coordination **scheme_1**, **scheme_2** and **scheme_3** respectively. For each scheme, the optimal coordination decision parameters are shown in bold and italics.

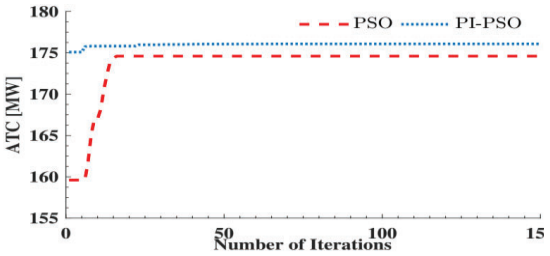

Fig. 6. Comparison of ATC enhancement with SSSC using PSO and PI-PSO for T4

TABLE III. Enhance ATC values with TCSC and SSSC

Trans ID	ATC [MW]			TCSC Solution		SSSC Solution		
	No FACTS	PI-PSO						
		With TCSC	With SSSC	Line no.	%Comp	Line no.	Vse (p.u)	dse(deg)
T1	143.2545	182.0445	166.5841	8(9 to 6)	80	6(8 to 9)	0.08809	158.753
T2	127.1567	153.8496	159.405	3(5 to 7)	46.6243	5(7 to 8)	0.0999	166.301
T3	118.0243	172.6364	143.0993	8(9 to 6)	76.0102	3(5 to 7)	0.05184	-76.74
T4	155.1414	181.0710	176.8958	3(5 to 7)	38.9587	5(7 to 8)	0.08255	84.9858
T5	138.6407	151.8797	152.7878	5(7 to 8)	57.2176	6(8 to 7)	0.0999	169.1835

TABLE IV. ATC ENHANCEMENT AND FACTS' PARAMETERS WITH **SCHEME_1**

Trans ID	ATC[MW]	TCSC		SSSC		
		Line no.	%Com	Line no.	Vse (p.u)	dse (deg)
T1	184.633	8(9 to 6)	***80***	6	***0.1***	***-165.4583***
T2	153.9241	3(5 to 7)	***21.23***	5	***0.1***	***132.9342***
T3	173.9017	8(9 to 6)	***54.295***	3	***0.1***	***-44.775***
T4	179.1634	3(5 to 7)	***22.7756***	5	***0.1***	***89.7476***
T5	154.7324	5(7 to 8)	***63.5491***	6	***0.1***	***-159.9218***

TABLE V. ATC ENHANCEMENT AND FACTS' PARAMETERS WITH **SCHEME_2**

Trans ID	ATC[MW]	TCSC		SSSC		
		Line no.	%Com	Line no.	Vse (p.u)	dse (deg)
T1	199.7187	8	80	***9***	***0.1***	***16.6043***
T2	162.346	3	46.6243	***4***	***0.1***	***134.9691***
T3	175.5847	8	76.0102	***6***	***0.1***	***161.818***
T4	182.2383	3	38.9587	***6***	***0.068976***	***-154.4956***
T5	154.6925	5	57.2176	***6***	***0.1***	***-166.0936***

TABLE VI. ATC ENHANCEMENT AND FACTS' PARAMETERS WITH **SCHEME_3**

Trans ID	ATC[MW]	TCSC		SSSC		
		Line no.	%Com	Line no.	Vse (p.u)	dse (deg)
T1	199.7187	8	***80***	***9***	***0.1***	***16.6063***
T2	163.2491	3	***45.5584***	***4***	***0.099905***	***133.5905***
T3	178.9711	8	***69.5688***	***4***	***0.1***	***107.7372***
T4	182.832	3	***57.0019***	***6***	***0.059166***	***160.8116***
T5	162.6633	5	***35.7543***	***4***	***0.1***	***120.0035***

Fig. 7 compares the convergence curve of transaction T3 for all coordination scheme using the proposed PI-PSO. From Tables IV, V and VI as well as Fig. 7, coordination **scheme_3** ensures superior ATC improvement. The higher number of iterations to convergence of **scheme_3** is attributable to the more number of decision parameters $(X_{TCSC}, \lambda_{SSSC}, X_{SSSC})$ required to be optimally tuned simultaneously.

Transfer capability improvement translates to increase loadability of a power system network. Consequently, Fig. 8 compares the nose curves of coordination schemes for transactions T1. As shown in Tables V and VI, as well as Fig. 8, coordination **scheme_2** and **scheme_3**, gives higher loadability margin compares to **scheme_1** and the base case without FACTS.

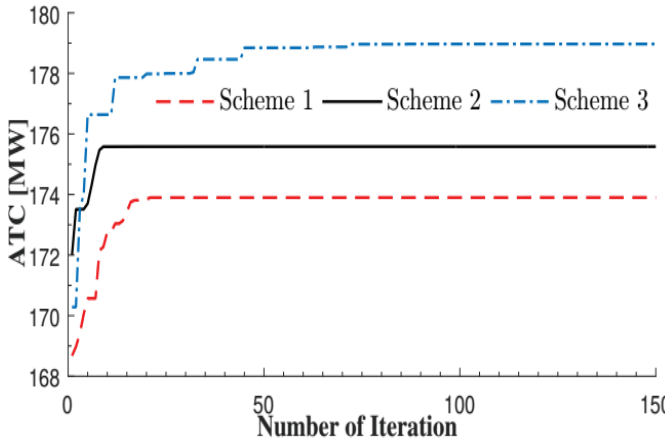

Fig. 7. Comparison of ATC by coordination schemes for transaction T3

To further demonstrate the success of the proposed PI-PSO, Fig. 9 compares the ATC by coordination **scheme_2** and **scheme_3** for an exhaustive search at all locations for transaction T5. Although both schemes follow the same pattern of ATC improvement at each location, **scheme_3** obtains higher improvement at line number 4, which is consistent with the results of Table 6. The Zero ATC value in line number 5 of Fig. 9 is as a result of non-placement of SSSC at the same location with an existing TCSC.

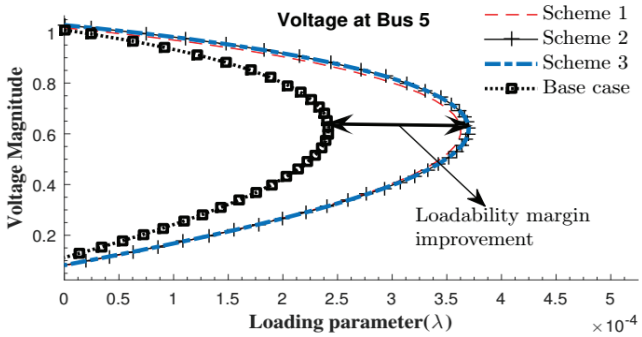

Fig. 8. Complete nose curves of transaction T1

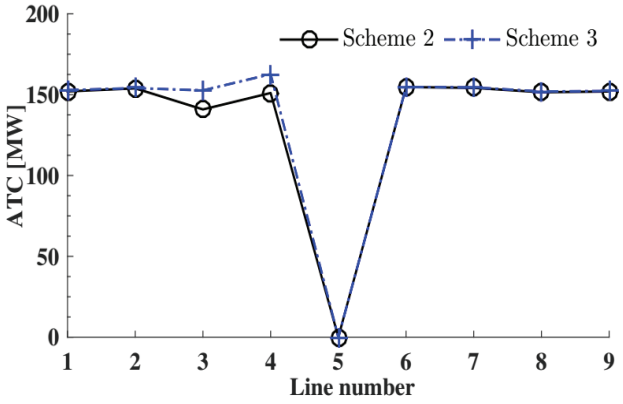

Fig. 9. Comparison of coordination schemes for transaction T5.

VIII. Conclusion

Optimal location and coordination of TCSC and SSSC is demonstrated using the proposed PI-PSO. Compare to conventional PSO, PI-PSO performs better regarding exploitation thereby improve starting point. The coordination scheme with a higher number of optimisation decision parameters gives superior ATC values with multi-type FACTS coordination. Although the power transfer directions considered were all constraints by line overloads at base case, future work intends to address transactions limited by bus voltage as well as examine the use of PI-PSO with (N – 1) contingency considerations.

References

[1] S. Sutha and N. Kamaraj, "Optimal Location of Multi Type Facts Devices for Multiple Contingencies Using Particle Swarm Optimization," *World Acad. Sci. Eng. Technol.*, vol. 16, no. 22, pp. 791–797, 2008.

[2] R. Surya, N. Janathanan, and S. Balamurugan, "A Novel Technique for Congestion Management in Transmission System by Real Power Flow Control," in *2017 International Conference on Intelligent Computing,Instrumentation and Control Technologies (ICICICT) ANovel*, 2017, pp. 1349–1354.

[3] P. P. Kulkarni and N. D. Ghawghawe, "Optimal Placement and Parameter setting of TCSC in Power Transmission System to increase the Power Transfer Capability," in *2015 International Conference on Energy Systems and Applications (ICESA 2015)*, 2015, no. Icesa, pp. 735–739.

[4] S. A. Mohamed, N. Luo, T. Pujol, and L. Pacheco, "Voltage Sourced Converter (VSC) based on multiple FACTS controllers for the improvement of power quality," *Renew. Energy Power Qual. J.*, vol. 1, no. 16, pp. 65–70, 2018.

[5] C. LI *et al.*, "Optimal allocation of multi-type FACTS devices in power systems based on power flow entropy," *J. Mod. Power Syst. Clean Energy*, vol. 2, no. 2, pp. 173–180, 2014.

[6] A. Elmitwally and A. Eladl, "Planning of multi-type FACTS devices in restructured power systems with wind generation," *Int. J. Electr. Power Energy Syst.*, vol. 77, pp. 33–42, 2016.

[7] S. Chansareewittaya and P. Jirapong, "Total transfer capability enhancement with optimal number of UPFC using hybrid TSSA," in *2012 9th International Conference on Electrical Engineering/Electronics, Computer, Telecommunications and Information Technology, ECTI-CON 2012*, 2012, pp. 1–7.

[8] T. Nireekshana, G. R. Kesava, and S. R. Sivanaga, "Available transfer capability enhancement with FACTS using Cat Swarm Optimization," *Ain Shams Eng. J.*, vol. 7, no. 1, pp. 159–167, 2016.

[9] R. M. Idris, A. Khairuddin, and M. W. Mustafa, "Optimal Allocation of FACTS Devices for ATC Enhancement Using Bees Algorithm," *Int. J. Electr. Comput. Energ. Electron. Commun. Eng.*, vol. 3, no. 6, pp. 1295–1302, 2009.

[10] S. Chansareewittaya and P. Jirapong, "Power transfer capability enhancement with optimal maximum number of facts controllers using evolutionary programming," in *IECON 2011 - 37th Annual Conference of the IEEE Industrial Electronics Society*, 2011, pp. 4733–4738.

[11] K. Bavithra, S. C. Raja, and P. Venkatesh, "Optimal Setting of FACTS Devices using Particle Swarm Optimization for ATC Enhancement in Deregulated Power System," *IFAC-PapersOnLine*, vol. 49, no. 1, pp. 450–455, 2016.

[12] S. Chansareewittaya, "Optimal allocation of Multi-type FACTS Controllers for Total Transfer Capability Enhancement Using Hybrid Particle Swarm Optimization," in *IEEE 2014 11th International Conference on Electrical Engineering/Electronics, Computer, Telecommunications and Information Technology (ECTI-CON) - Nakhon Ratchasima, Thailand*, 2014, pp. 1–6.

[13] V. Srinivasa, Rao and R. S. Rao, "Comparison of various methods for optimal placement of FACTS devices," in *International Conference on Smart Electric Grid (ISEG), 2014*, 2014, no. 1, pp. 1–7.

[14] M. Ebeed, S. Kamel, and F. Jurado, "Constraints violation handling of SSSC with multi-control modes in Newton–Raphson load flow algorithm," *IEEJ Trans. Electr. Electron. Eng.*, vol. 12, no. 6, pp. 861–866, 2017.

[15] M. Balasubbareddy, S. Sivanagaraju, and C. Venkata, "A Non-Dominated Sorting Hybrid Cuckoo Search Algorithm for Multi-Objective Optimization in the Presence of FACTS Devices," *Russ. Electr. Eng.*, vol. 88, no. 1, pp. 44–53, 2017.

[16] S. Manikandan and P. Arul, "Optimal Location of Multiple FACTS Device Using Sensitivity Methods," *Int. J. Eng. Trends Technol. –*, vol. 4, no. 10, pp. 4361–4367, 2013.

[17] R. Yao, F. Liu, G. He, B. Fang, and L. Huang, "Static security region calculation with improved CPF considering generation regulation," in *2012 IEEE International Conference on Power System Technology, POWERCON 2012*, 2012, pp. 1–6.

[18] X. Dou *et al.*, "An improved CPF for static stability analysis of distribution systems with high DG penetration," *Int. J. Electr. Power Energy Syst.*, 2016.

[19] M. Khosravifard and M. Shaaban, "Risk-based available transfer capability assessment including nondispatchable wind generation," *Int. Trans. Electr. Energy Syst.*, vol. 25, no. 11, pp. 3169–3183, 2015.

[20] C. K. Babulal and P. S. Kannan, "A Novel Approach for ATC Computation in Deregulated Environment," *J. Electr. Syst*, vol. 2, no. 3, pp. 146–161, 2006.

[21] R. Prathiba *et al.*, "Multiple output radial basis function neural network with reduced input features for on-line estimation of available transfer capability," *Control Eng. Appl. Informatics*, vol. 18, no. 1, pp. 95–106, 2016.